Electrochemical Chaos Control in a Chemical Reaction: Experiment and Simulation

A. Guderian, A. F. Münster, M. Kraus, and F. W. Schneider*

Institute of Physical Chemistry, University of Würzburg, Am Hubland, 97074 Würzburg, Germany

Received: February 4, 1998; In Final Form: April 6, 1998

On the basis of previous theoretical work we present a simple method of chaos control in experiment and simulation using the Belousov−Zhabotinsky (BZ) reaction. The chaos control parameter employed is the sinusoidally modulated electric current (AC) acting on a Pt-working electrode. The experimental chaos control takes place in the well-known low flow rate region of the BZ reaction in a CSTR (continuous flow stirred tank reactor). It was possible to stabilize several unstable periodic orbits (UPO) in the BZ experiment, namely P1, P2, P3, and P4. The chosen model of chemical chaos is the seven-variables model (Montanator) of Györgyi and Field. The stabilized UPO (P3) in the model calculations is compared to the same UPO stabilized by time-delayed feedback method according to Pyragas. In addition we use the continuous time-delayed feedback method to achieve the tracking of the UPO starting in the chaotic range and continuing beyond.

1. Introduction

Chaos control stands for the stabilization of an unstable periodic orbit (UPO) contained in a strange attractor. A chaotic attractor consists of a large number of UPOs which may be stabilized by various available control methods.[1−17] In chemical reactions only few UPOs can be usually found and stabilized in experiment and numerical simulations. An important chaos control technique has been developed by Ott, Grebogi, and Yorke (OGY).[18] The OGY method applies small time-dependent perturbations to the system requiring a simultaneous on-line computer analysis. This discontinuous chaos control method has been applied to a number of physical[19−25] and chemical systems, including the BZ reaction.[26,27] Another chaos control method is the continuous time-delayed feedback method developed by Pyragas,[28,29] which we applied to chaos in the enzymatic peroxidase-oxidase reaction,[30] to the experimental BZ system,[31] and to the seven-variables−Montanator model.[31,33,34] Recently a resonant chaos control method[3−8] has been applied to the seven-variables−Montanator model,[32] where a chaotic motion is converted into a periodic motion by imposing one or more sinusoidal flow rate perturbations. The frequencies, phases, and amplitudes of the driving functions are adjusted appropriately. The latter method of chaos control works without feedback, and it should be very convenient in its experimental use, since on-line registration and control of the actual reaction concentrations is not necessary. The experimental system chosen in this work is the BZ reaction which is run in a CSTR at low flow rate.[35−39] Instead of a flow rate perturbation, as described in previous work,[32] we use an electrical perturbation in this study. We show experimentally that the stabilized UPOs are part of the chaotic attractor and that they have not been generated by the interaction with the external perturbation. In the simulations we also apply a tracking method of periodic orbits[40] which is based on the time-delayed feedback by Pyragas, in order to show that the UPOs stabilized by time-delayed feedback are completely embedded in the chaotic attractor.[28,29]

* To whom correspondence should be addressed.

2. Experimental Setup

2.1. Materials. Malonic acid (Merck) was recrystallized twice from acetone to remove trace impurities.[36−38] Sulfuric acid, cerous sulfate (Riedel-de-Haën), and potassium bromate (Merck) were of analytical grade and used without further purification. The water was purified by ion exchange (water purification system Milli-Q, Millipore; specific resistance ≥10 MΩ cm). All solutions were equilibrated with air.

2.2. Reactor. The experimental setup is presented in Figure 1. Both reactors contain a Pt-working electrode with a surface of 3.0 cm^2. The right reactor (Figure 1, 3.24 mL) is fed with the BZ solutions and contains a Pt/Ag/AgCl−redox electrode−chain (Ingold) to monitor the redox potential. Due to inevitable variations in the sensitivity of the reference electrode, the output signal is recorded in arbitrary units. The solutions are mixed efficiently with a Teflon stirrer at a stirring rate of 1400 rpm. The left reactor (Figure 1) containing the Pt counter electrode is filled with 0.6 M sulfuric acid. It is not necessary to flow the H_2SO_4 solution into the reactor, since its concentration does not change significantly during a given experiment. Both reactors are separated by a teflon membrane with pore size of 1−2 μm. The CSTR (right) is fed by a three-channel syringe pump containing the reactant solutions. The latter is controlled by a laboratory computer via a DA converter. The educts enter the reactor in three separate feedlines through the bottom. The reactant solutions are as follows: syringe 1, 0.3 M $KBrO_3$; syringe 2, 1.25×10^{-3} M $Ce_2(SO_4)_3$; syringe 3, 0.75 malonic acid and 0.6 M H_2SO_4.[39] To obtain reactor concentrations, divide by three. The two reactors, the feedlines, and the syringes are thermostated at 26 ± 0.2 °C.

2.3. Continuous Flow Conditions. Under these experimental conditions chaos appears at a flow rate of $k_f^{(1)} = 4.58 \times 10^{-4}$ s^{-1} corresponding to a residence time of $\tau = 36.4$ min (Figure 2a). Chaos is reached through a period doubling route by lowering the flow rate.[39] The given value of the flow rate ($k_f^{(1)}$) refers to the center of the chaotic region. Further measurements were performed at flow rates of $k_f^{(2)} = 4.37 \times 10^{-4}$ s^{-1} ($\tau = 38.2$ min) (Figure 4a), which is 5% below $k_f^{(1)}$,

S1089-5639(98)00997-9 CCC: $15.00
Published on Web 06/05/1998

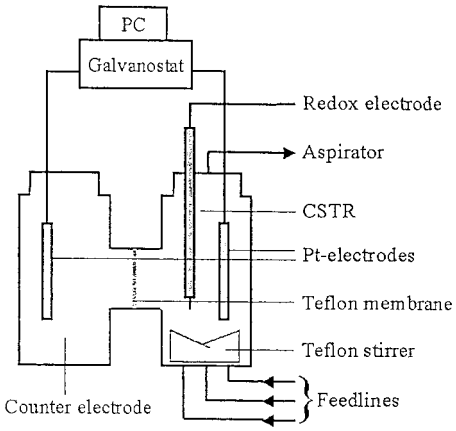

Figure 1. CSTR (3.24 mL volume): The sinusoidal electric perturbation is applied via the Pt electrodes connected to a galvanostat. The redox potential is measured using a Pt/Ag/AgCl redox electrode.

and $k_f^{(3)} = 5.01 \times 10^{-4}$ s^{-1} ($\tau = 33.2$ min) (Figure 4b) which is 9% above $k_f^{(1)}$.

2.4. Electrical Perturbation. The electrical sinusoidal perturbation of the reaction is realized by the two Pt electrodes connected to a galvanostat (EG&G) which is controlled by a laboratory computer via a DA converter. The imposed alternating current I [mA] is given by eq 1, where I_0 is the amplitude of the alternating current and ν_P the modulation (perturbation) frequency [Hz]:

$$I = I_0 \sin(2\pi\nu_P t) \propto \frac{d[Ce^{(IV)}]}{dt} \qquad (1)$$

Thus the current as well as the perturbing potential alternates between positive and negative values. According to Vetter,[41] there are no inhibiting polarization processes for the Ce(III)/Ce(IV) redox couple. We conclude also from our previous work that other redox processes involving bromine species occur, but they can be neglected.[42,43]

2.5. Data Evaluation. For all stabilized orbits we compute the Fourier spectra and compare them with the Fourier spectrum of the unperturbed chaotic time series. In order to check if the stabilized orbit is embedded in the strange attractor, we used the Takens method for attractor reconstruction from the measured time series.[44] The singular value decomposition (SVD) method, which is generally more reliable for evaluation of invariant measures, could not be used in this case because of the coordinate transformation involved in the attractor reconstruction.[45] The experimental time series of 2000 data points were recorded with a sampling rate of 1 Hz.

2.6. Experimental Results. The capacity dimension of the strange attractor observed at $k_f^{(1)}$ is $D_H = 2.3$ (calculated with nearest-neighbor analysis).[46−48] The reconstruction of the attractor for the dimensional analysis was performed using the SVD method.[45]

In the following the period of the alternating current is T_P. The main frequency of the system's response is called ν_R, and the corresponding period is T_R. The perturbation amplitude was chosen to be $I_0 = 0.02$ mA for all experiments leading to an amplitude for the potential of $U_0 = 1.1$ V. The periodic perturbation according to eq 1 was started after 6−7 residence times of free running chaos. The perturbation frequency was $\nu_P = 1.72 \times 10^{-2}$ Hz ($T_P = 58$ s) corresponding to the major peak in the Fourier spectrum of the chaotic times series (Figure 3a). A P2 orbit could be stabilized (Figure 2b and power spectrum Figure 3b). Its frequency was $\nu_R = 8.47 \times 10^{-3}$ Hz

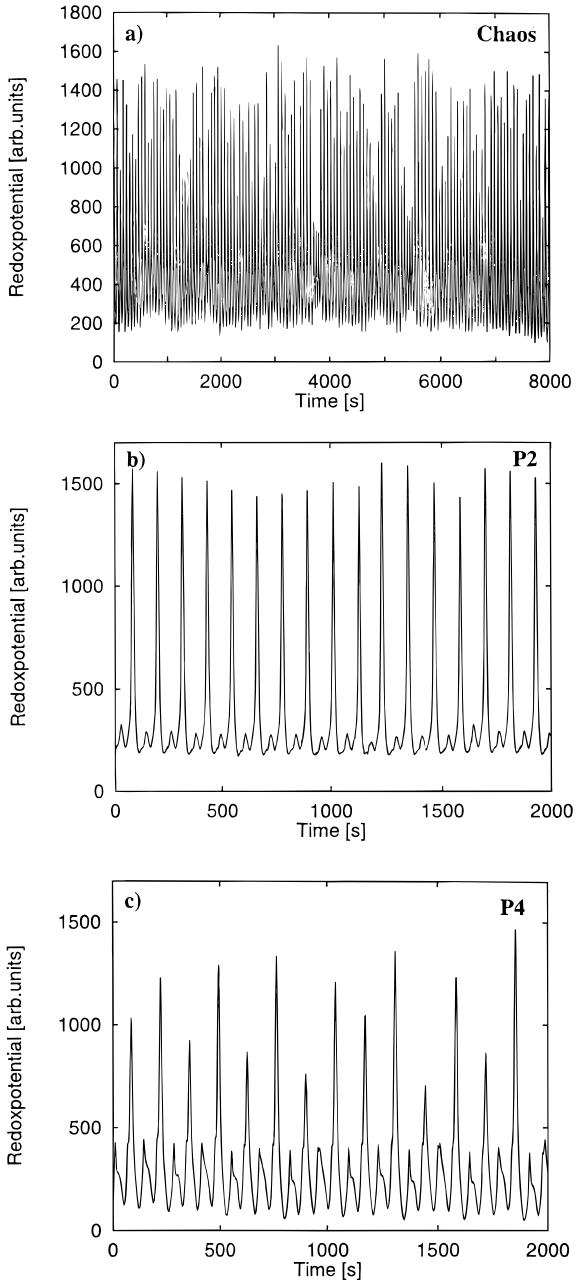

Figure 2. (a) Time series of experimental chaos at a flow rate of $k_f^{(1)} = 4.58 \times 10^{-4}$ s^{-1} ($\tau = 36.4$ min). (b) Experimental time series of the stabilized P2 orbit. The perturbation was realized by using alternating current with a frequency $\nu_P = 1.72 \times 10^{-2}$ Hz ($T_P = 58$ s) and an amplitude of $I_0 = 0.02$ mA. The stabilized P2 orbit had a frequency of $\nu_R = 8.47 \times 10^{-3}$ Hz ($T_R = 118$ s). (c) Experimental time series of the stabilized P4 orbit. The perturbation was realized by using alternating current with a frequency of $\nu_P = 1.47 \times 10^{-2}$ Hz ($T_P = 68$ s) and an amplitude of $I_0 = 0.02$ mA. Its frequency was $\nu_R = 3.64 \times 10^{-3}$ Hz ($T_R = 275$ s).

($T_R = 118$ s). The relation between ν_P and ν_R is 2:1. If the perturbation frequency was decreased from $\nu_P = 1.72 \times 10^{-2}$ Hz ($T_P = 58$ s) to $\nu_P = 8.47 \times 10^{-3}$ Hz ($T_P = 118$ s), we obtained the same P2 orbit ($\nu_R = 84.7 \times 10^{-3}$ Hz) (not shown); which is a frequency relation of 1:1. With a perturbation frequency of $\nu_P = 1.47 \times 10^{-2}$ Hz ($T_P = 68$ s) the chaotic motion was controlled to become a P4 orbit (2^2) (L^S = large and small amplitudes) with $\nu_R = 3.64 \times 10^{-3}$ Hz ($T_R = 275$ s) (Figure 2c and power spectrum Figure 3c). Here ν_P:ν_R is 4:1. In another chaos control measurement under the same perturbation conditions the system responded with a P3 orbit (1^2) of ν_R

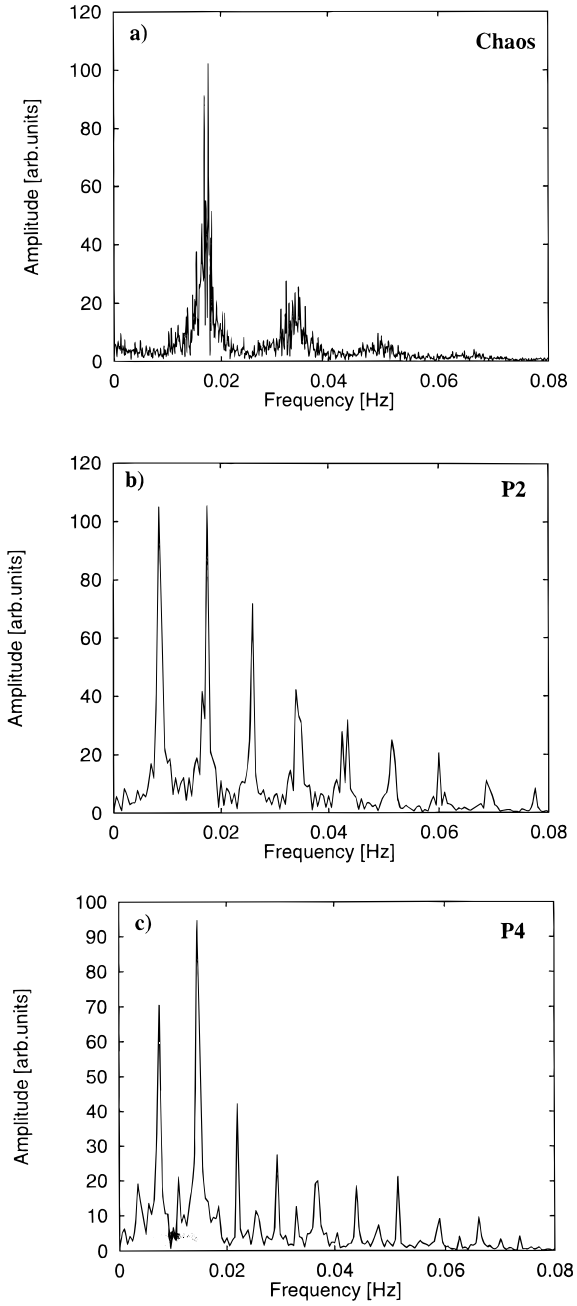

Figure 3. (a) Fourier spectrum of the experimental chaotic time series with a major peak of $\nu = 1.72 \times 10^{-2}$ Hz ($T_P = 58$ s). (b) Fourier spectrum of the experimental P2 orbit. (c) Fourier spectrum of the experimental P4 orbit.

$= 7.35 \times 10^{-3}$ Hz ($T_R = 136$ s) (not shown); here ν_P:ν_R is 2:1. Increasing the perturbation frequency to $\nu_P = 2.08 \times 10^{-2}$ Hz ($T_P = 48$ s) enables the stabilization of another P2 orbit, which had a frequency of $\nu_R = 1.04 \times 10^{-2}$ Hz ($T_R = 96$ s) (not shown). Here the frequency relation is 2:1.

In another set of experiments we lowered the flow rate to $k_f^{(2)} = 4.37 \times 10^{-4}$ s^{-1} and applied the same perturbation procedures as above for $\nu_P = 1.72 \times 10^{-2}$ Hz. Here the major peak frequency of the chaotic Fourier spectrum, namely 1.72×10^{-2} Hz, is the same as above. We now obtained a P3 orbit with $\nu_R = 5.75 \times 10^{-3}$ Hz ($T_R = 174$ s) (Figure 4a and power spectrum Figure 5a) instead of the P2 orbit observed at $k_f^{(1)}$. The frequency relation is 3:1. For further chaos control experiments we raised the flow rate to $k_f^{(3)} = 5.01 \times 10^{-4}$ s^{-1} and applied the same perturbation. In the latter case the system

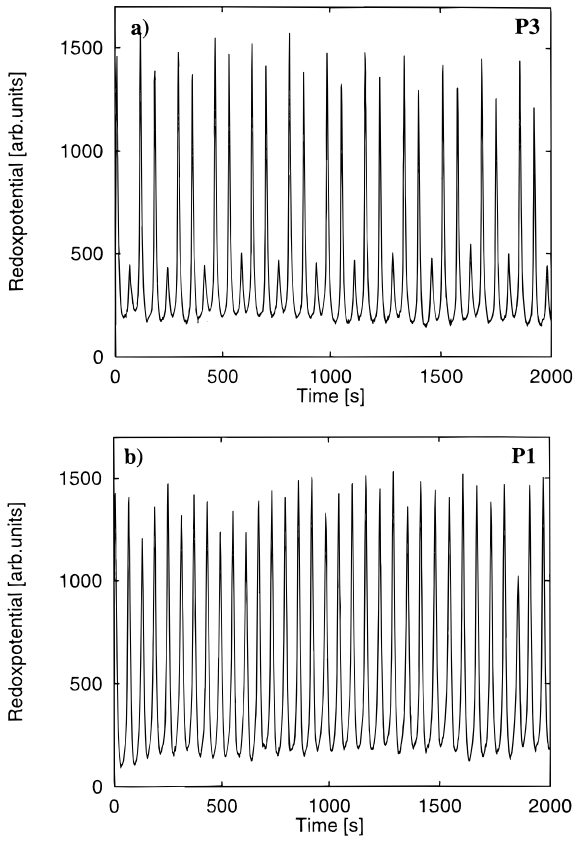

Figure 4. (a) Experimental time series of the P3 orbit at a constant flow rate of $k_f^{(2)} = 4.37 \times 10^{-4}$ s^{-1} ($\tau = 38.2$ min). The perturbation frequency was $\nu_P = 1.72 \times 10^{-2}$ Hz ($T_P = 58$ s), and the frequency of the stabilized orbit was $\nu_R = 5.75 \times 10^{-3}$ Hz ($T_R = 174$ s). (b) Experimental time series of the P1 orbit at a constant flow rate of $k_f^{(3)} = 5.01 \times 10^{-4}$ s^{-1} ($\tau = 33.2$ min). The perturbation frequency was $\nu_P = 1.72 \times 10^{-2}$ Hz ($T_P = 58$ s), and the frequency of the stabilized orbit was $\nu_R = 1.66 \times 10^{-2}$ Hz ($T_R = 60$ s).

stabilized in a P1 orbit with $\nu_R = 1.66 \times 10^{-2}$ Hz ($T_R = 60$ s) (Figure 4b and power spectrum Figure 5b). The frequency relation is 1:1.

3. Model Calculations with the Seven-Variables−Montanator Model

In order to simulate the low flow rate chaos of the experimental BZ system we used the seven-variables−Montanator model.[33,34] The Montanator model consists of two autocatalytic cycles, one containing the production of $HBrO_2$ by the reduction of bromate with cerium(III); the second autocatalytic cycle represents the formation of bromide from bromomalonic acid. The mechanism and the rate constants of the seven-variables−Montanator are given in Tables 1 and 2. The following species are used as the variables in the model: bromous acid, bromide, bromate, bromomalonic acid, bromomalonic acid radical, cerium(III), and cerium(IV). The model is in good agreement with the experimentally observed deterministic chaos. An external electric current corresponding to oxidation and reduction of the Ce(III)/Ce(IV) couple is included in the model:

$$\frac{d[Ce^{(III)}]}{dt} = S([Ce^{(III)}]) - k_f([Ce^{(III)}] - [Ce^{(III)}]_0) + j \quad (2)$$

$$\frac{d[Ce^{(IV)}]}{dt} = S([Ce^{(IV)}]) - k_f([Ce^{(IV)}]) - j \quad (3)$$

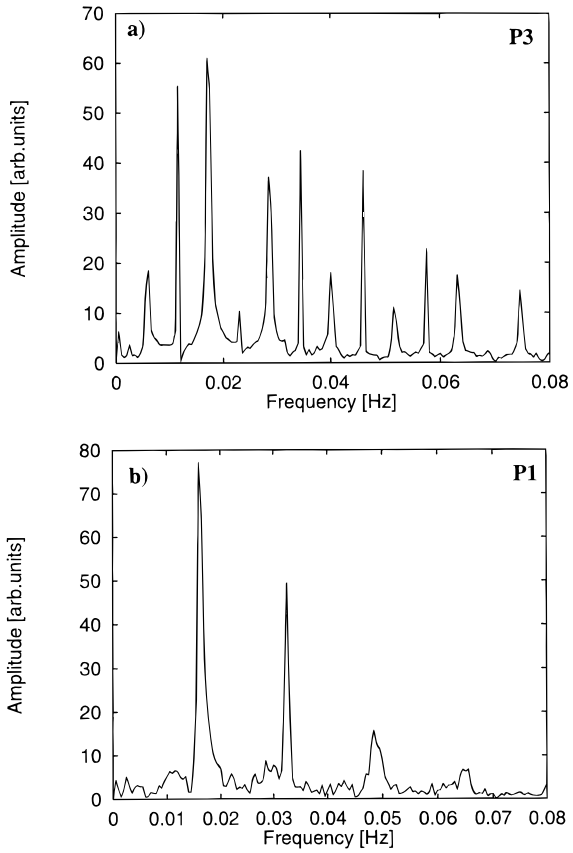

Figure 5. (a) Fourier spectrum of the experimental P3 orbit. (b) Fourier spectrum of the experimental P1 orbit.

TABLE 1: Seven-Variables−Montanator Model (Nonstoichiometric Steps)[a]

$Br^- + HBrO_2 + H^+ \rightarrow 2BrMA$	(R1)
$Br^- + BrO_3^- + 2H^+ \rightarrow BrMA + HBrO_2$	(R2)
$2HBrO_2 \rightarrow BrO_3^- + BrMA + H^+$	(R3)
$BrO_3^- + HBrO_2 + H^+ \rightarrow 2BrO_2^\bullet + H_2O$	(R4)
$2BrO_2^\bullet + H_2O \rightarrow BrO_3^- + HBrO_2 + H^+$	(R5)
$Ce^{3+} + BrO_2^\bullet + H^+ \rightarrow HBrO_2 + Ce^{4+}$	(R6)
$HBrO_2 + Ce^{4+} \rightarrow Ce^{3+} + BrO_2^\bullet + H^+$	(R7)
$MA + Ce^{4+} \rightarrow MA^\bullet + Ce^{3+} + H^+$	(R8)
$BrMA + Ce^{4+} \rightarrow Ce^{3+} + Br^-$	(R9)
$MA^\bullet + BrMA \rightarrow MA + Br^-$	(R10)
$2MA^\bullet \rightarrow MA$	(R11)

[a] MA = malonic acid; MA• = malonic acid radical; BrMA = bromomalonic acid.

TABLE 2: Rate Constants and Concentrations of the Seven-Variables−Montanator Model

k_{R1}	2.0×10^6 s^{-1} M^{-2}	k_{R8}	3.0×10^{-1} s^{-1} M^{-1}
k_{R2}	2.0 s^{-1} M^{-3}	k_{R9}	3.0×10^1 s^{-1} M^{-1}
k_{R3}	3.0×10^3 s^{-1} M^{-1}	k_{R10}	2.4×10^4 s^{-1} M^{-1}
k_{R4}	3.3×10^1 s^{-1} M^{-2}	k_{R11}	3.0×10^9 s^{-1} M^{-1}
k_{R5}	7.6×10^5 s^{-1} M^{-2}	$[BrO_3^-]$	0.1 M
k_{R6}	6.2×10^4 s^{-1} M^{-2}	$[H_2O]$	55 M
k_{R7}	7.0×10^3 s^{-1} M^{-1}	$[H^+]$	0.26 M

$$j = j_0 \sin(2\pi\nu_P t) \tag{4}$$

$$j_0 = -\chi\nabla\phi \tag{5}$$

$$\chi = F\cdot u(Ce^{(IV)})[Ce^{(IV)}] \tag{6}$$

The CSTR is assumed to be well-stirred, and any concentration gradients are neglected. $S([Ce^{(III)}])$ is the chemical source term for Ce(III) and represents the chemical reaction rates; j is the electric current density contributed by Ce(IV), j_0 is the amplitude of the alternating current. ν is the frequency [Hz], χ is the contribution of the Ce(IV) to the conductivity, $\nabla\phi$ is the electrical potential gradient, F is the Faraday constant, and u is the mobility of Ce(IV) ions. We combine the constant factors F, u, and $\nabla\phi$ to obtain the parameter C_0, which is directly correlated with the amplitude j_0.

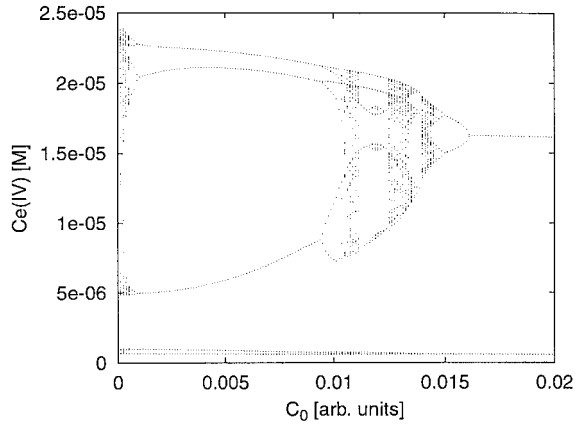

Figure 6. Montanator model: Bifurcation diagram with direct current applied on the low flow rate chaos of the BZ system ($k_f = 3.0 \times 10^{-4}$ s^{-1} ($\tau = 55.5$ min)).

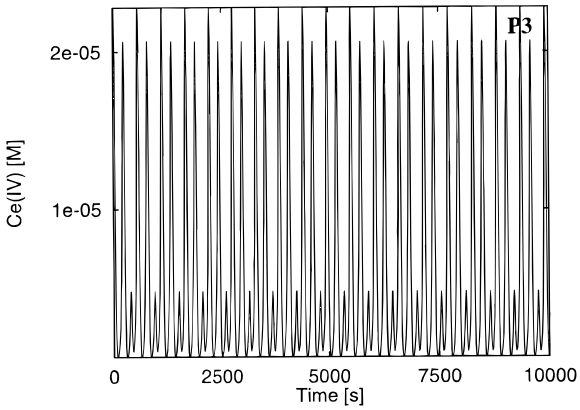

Figure 7. Montanator model: Time series of the stabilized P3 orbit obtained at a constant flow rate of $k_f = 3.0 \times 10^{-4}$ Hz ($\tau = 55.5$ min) and a perturbation frequency of $\nu_P = 7.27 \times 10^{-3}$ Hz ($T_P = 137.5$ s) and an amplitude of $C_0 = 0.001$. The P3 had a frequency of $\nu_R = 1.82 \times 10^{-3}$ Hz ($T_R = 550$ s).

$$C_0 = -F\cdot u\cdot\nabla\phi \tag{7}$$

The resulting ordinary differential equations were numerically integrated using the Gear method. The flow rate is set to $k_f = 3.0 \times 10^{-4}$ s^{-1}. The bifurcation diagram with C_0 as the bifurcation parameter shows P1 oscillations for $C_0 = 1.62 \times 10^{-2}$ (Figure 6). When the value of the bifurcation parameter was lowered, the system displays P2 oscillations through period doubling into a chaotic region with a $D_C = 2.3$ (capacity dimension) of the attractor. By lowering the ac amplitude to $C_0 < 1.0 \times 10^{-2}$, P3 oscillations were obtained. They disappeared at an amplitude of $C_0 = 5.0 \times 10^{-4}$ and gave way to a narrow region of chaos via period doubling (Feigenbaum route).

3.1. Simulation of Chaos Control. A flow rate of $k_f = 3.0 \times 10^{-4}$ s^{-1} was maintained in all simulations. The perturbation frequencies were derived from the Fourier spectrum of the uncontrolled chaos (Figure 8a). With a perturbation frequency of $\nu_P = 7.27 \times 10^{-3}$ Hz and an amplitude of $C_0 = 0.001$ a P3 oscillation (2^1) with a main frequency of $\nu_R = 1.82 \times 10^{-3}$ Hz

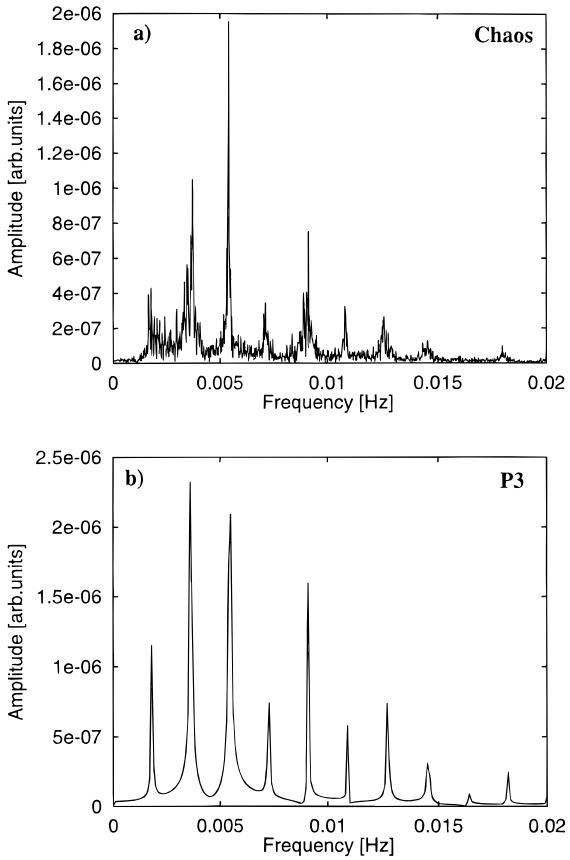

Figure 8. (a) Montanator model: Fourier spectrum of the low flow rate chaos ($k_f = 3.0 \times 10^{-4}$ s^{-1} ($\tau = 55.5$ min)). (b) Montanator model: Fourier spectrum of the stabilized P3 orbit.

is stabilized (Figure 7). Here the ratio ν_P:ν_R equals 4. An identical P3 pattern has been stabilized for additional perturbation frequencies where $\nu_P = n\nu_R$, namely $\nu_P' = 1.09 \times 10^{-2}$ Hz and $\nu_P'' = 2.18 \times 10^{-2}$ Hz, for $n = 6$ and 12, respectively. The latter frequencies, however, required a higher value of the amplitude, namely $C_0 = 0.002$, in order to stabilize the P3 orbit. Thus, the amplitudes of the various perturbation frequencies (for different stabilized UPOs) are not identical.

3.2. Tracking. We used a delayed-feedback based method to show that the stabilized P3 orbit is an UPO contained in the strange attractor.[40] If the period (τ) of the stabilized UPO and the coupling strength (A in eq 8) are known, the UPO can be tracked through the chaotic region. For the tracking of the P3 orbit the bifurcation parameter C_0 (eq 7) is varied while the Pyragas-type control remains active.

$$\frac{d[HBrO_2]}{dt} = S[HBrO_2] - k_f[HBrO_2] + A([HBrO_2](t-\tau) - [HBrO_2](t)) \quad (8)$$

The balance equations of the Ce(III)/Ce(IV) couple were treated as shown in eqs 2−6. Figure 9 shows the bifurcation diagram for $A = 0$ together with the results of the tracking method as described before (diamonds in Figure 9). The delay time was $\tau = 550$ s, the required Pyragas feedback amplitude was found to be $A = 0.001$, and the AC perturbation was $\nu_P = 7.27 \times 10^{-3}$ Hz ($T_P = 137.5$ s).

4. Discussion and Conclusions

We demonstrate a simple and efficient way to control chaos in the experimental BZ system and in the numerical simulations

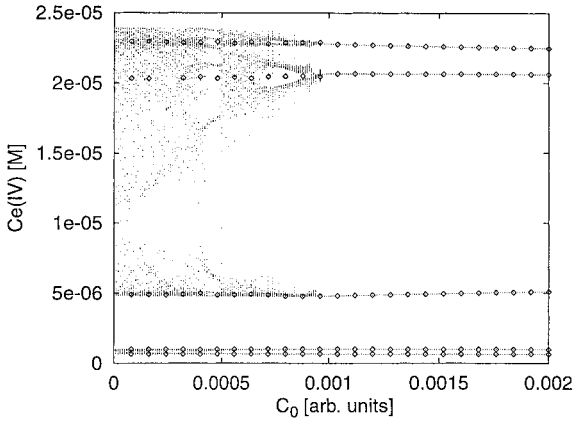

Figure 9. Montanator model: Combined bifurcation diagram with alternating current applied to the chaotic BZ system (dots) and alternating current applied together with the continuous feedback control (diamonds) (tracking method). The perturbation frequency was $\nu_P = 7.27 \times 10^{-3}$ Hz ($T_P = 137.5$ s), and the delay time used for tracking was $\tau = 550$ s.

of the 7-variables−Montanator model. In experimental chaos control, the major frequency of the chaotic Fourier spectrum was used as the perturbation frequency. In the center of the chaotic range an orbit of period two could be stabilized. We also stabilized P2, P4, and P3 orbits by changing the perturbation frequency. The ratio ν_P:ν_R was always a rational number equal to one or larger. If the flow rate is moved toward a neighboring periodic window, different periodic orbits can be stabilized: With a flow rate closer to the P3 region, the stabilized UPO is a P3. Here the relation between the perturbation and the response frequency was also a multiple (three) of the frequency of the stabilized periodic orbit. Similar results were obtained for the case with the flow rate closer to the P1 region, where the perturbation frequency equals the frequency of the response P1. These experiments confirm that it is possible to stabilize several different UPOs of a given chaotic attractor by electrochemical periodic perturbations. The type of UPO which is stabilized is the UPO which is the least unstable. In general, the corresponding stable orbit will be found in the close neighborhood of the chaotic attractor.[32]

In analogy to the continuous chaos control method proposed by Pyragas the inclusion of a sinusoidal ac perturbation expands the dimension of the low dimensional chemical system. The stabilization is achieved through those additional degrees of freedom which cause a decrease of the largest Lyapunov exponent of the UPO.[28,29]

The model calculations with the 7-variables−Montanator model differ from the experimental results only with respect to the perturbation frequencies. The most efficient stabilization of P3 was obtained by using the ν_P:ν_R ratio of 1:4. Ac frequencies of six times and 12 times the main frequency of the stabilized UPO control may also be used. Tracking of the P3 orbit clearly showed that this orbit is embedded in the original chaotic attractor.

Acknowledgment. We thank the Deutsche Forschungsgemeinschaft for partial financial support. We also thank Dr. G. Dechert and Dr. A. Förster for their technical support and valuable discussions.

References and Notes

(1) Hübler, A. W. *Helv. Phys. Acta* **1989**, *62*, 343.
(2) Hübler, A. W.; Georgii, R.; Kuchler, W.; Stebel, W.; Lüscher, E. *Helv. Phys. Acta* **1989**, *61*, 203.

(3) Hübler, A. W.; Lüscher, E. *Naturwissenschaften* **1989**, *76*, 67.
(4) Eisenhammer, T.; Hübler, A. W.; Geisel, A.; Lüscher, E. *Phys. Rev.* **1990**, *A41*, 3332.
(5) Chang, K.; Kodogeorgiou, A.; Hübler, A. W.; Jackson, E. A. *Physica* **1991**, *D51*, 99.
(6) Lance, E.; Hübler, W. A. *Phys. Rev.* **1994**, *E51*, 3561.
(7) Mettin, R.; Lauterborn, W.; Hübler, A. W.; Scheeline, A. *Tech. Rep. Keio Phys.* **1994**, *2*, 1.
(8) Mettin, R.; Kurz, T. *Phys. Lett.* **1995**, *A206*, 331.
(9) Singer, J.; Wang, Y. Z.; Bau, H. H. *Phys. Rev. Lett.* **1991**, *66*, 1123.
(10) Minh, D. V. *Phys. Rev. E* **1993**, *47*, 714.
(11) Genesio, R.; Tesi, A. *Automatica* **1992**, *28*, 531.
(12) Braiman, Y.; Goldhirsch, I. *Phys. Rev. Lett.* **1991**, *66*, 2545.
(13) Azevedo, A.; Rezende, S. M. *Phys. Rev. Lett.* **1991**, *66*, 1342.
(14) Fahy, S.; Hahmann, D. R. *Phys. Rev. Lett.* **1992**, *69*, 761.
(15) Stone, E. F. *Phys. Lett. A* **1992**, *163*, 367.
(16) Fowler, T. B. *IEEE Trans. Autom. Control* **1989**, *34*, 201.
(17) Mathias, M. A.; Güemez, R. *Phys. Rev. Lett.* **1993**, *72*, 1455.
(18) Ott, E.; Grebogi, C.; Yorke, J. A. *Phys. Rev. Lett.* **1990**, *64*, 1196.
(19) Romeiras, F. J.; Grebogi, C.; Ott, E.; Dayawansa, W. P. *Physica* **1992**, *58D*, 165.
(20) Roy, R.; Murphy, T. W.; Maier, T. D.; Gills, Z.; Hunt, E. R. *Phys. Rev. Lett.* **1992**, *68*, 1259.
(21) Gills, Z.; Iwata, C.; Roy, R.; Schwartz, I. B.; Triandaf, I. *Phys. Rev. Lett.* **1992**, *69*, 3169.
(22) Hunt, E. R. *Phys. Rev. Lett.* **1991**, *67*, 1953.
(23) Ditto, W. L.; Rauseo, S. N.; Spano, L. M. *Phys. Rev. Lett.* **1990**, *65*, 3211.
(24) Garfinkel, A.; Spano, M. L.; Ditto, W. L.; Weiss, J. N. *Science* **1992**, *257*, 1230.
(25) Hübinger, B.; Dörner, R.; Martienssen, W. *Z. Phys.* **1993**, *B90*, 103.
(26) Peng, B.; Petrov, V.; Showalter, K. J. *J. Phys. Chem.* **1991**, *95*, 4957.
(27) Petrov, V.; Gaspar, V.; Masere, J.; Showalter, K. J. *Nature* **1993**, *361*, 240.
(28) Pyragas, K. *Phys. Lett. A* **1992**, *170*, 421.
(29) Pyragas, K. *Z. Naturforsch.* **1993**, *48A*, 629.
(30) Lekebusch, A.; Förster, A.; Schneider, F. W. *J. Phys. Chem.* **1995**, *99*, 681.
(31) Schneider, F. W.; Blittersdorf, R.; Förster, A.; Hauck, T.; Lebender, D.; Müller, J. *J. Phys. Chem.* **1993**, *97*, 12244.
(32) Kraus, M.; Müller, J.; Lebender, D.; Schneider, F. W. *Chem. Phys. Lett.* **1996**, *260*, 51.
(33) Györgyi, L.; Field, R. J. *J. Phys. Chem.* **1991**, *95*, 6594.
(34) Györgyi, L.; Field, R. J. *Nature* **1992**, *355*, 808.
(35) Noszticzius, Z.; McCormick, W. D.; Swinney, H. L. *J. Phys. Chem.* **1987**, *91*, 5129.
(36) Coffman, K. G.; McCormick, W. D.; Noszticzius, Z.; Simoyi, R. H.; Swinney, H. L. *J. Chem. Phys.* **1987**, *86*, 119.
(37) Györgyi, L.; Field, R. J.; Noszticzius, Z.; McCormick, W. D.; Swinney, H. L. *J. Phys. Chem.* **1992**, *96*, 1228.
(38) Noszticzius, Z.; McCormick, W. D.; Swinney, H. L. *J. Phys. Chem.* **1989**, *93*, 2796.
(39) Schneider, F. W.; Münster, A. F. *J. Phys. Chem.* **1991**, *95*, 2130.
(40) Delgado, E. J.; Münster, A. F.; Schneider, F. W. *Ber. Bunsen-Ges. Phys. Chem.* **1995**, *99*, 1049.
(41) Vetter, K. J. *Z. Phys. Chem.* **1950**, *196*, 360.
(42) Dechert, G.; Schneider, F. W. *J. Phys. Chem.* **1994**, *98*, 3927.
(43) Zeyer, K.-P. W.; Dechert, G.; Hohmann, W.; Blittersdorf, R.; Schneider, F. W. *Z. Naturforsch.* **1994**, *49A*, 953.
(44) van der Water, W.; Schram, P. *Phys. Rev. A* **1988**, *37*, 3118.
(45) Badii, R.; Politi, X. *Phys. Rev. Lett.* **1984**, *52*, 1661.
(46) Gear, C. W. *Numerical initial value problems in ordinary differential equations*; Prentice Hall: Englewood Cliffs, NJ, 1971.
(47) Shampine, L. F.; Gear, C. W. *SIAM Rev.* **1979**, *21*, 1.
(48) Takens, F. *Lecture Notes in Mathematics*; Springer: Berlin, 1981; p 898.
(49) Broomhead, D. S.; King, G. P. *Physica D* **1986**, *20*, 217.
(50) Renyi, A. *Probability Theory*; North Holland: Amsterdam, 1970.